动态感应加热消除轨面堆焊热影响区马氏体组织

宄文涛， 李晓延， 李 辉， 孙建通
(北京工业大学 材料科学与工程学院，北京 100124)

摘 要：采用动态感应加热的方法消除了U71Mn钢轨轨面堆焊后热影响区的马氏体组织. 通过光学显微组织分析和显微硬度测试对马氏体组织的消除效果进行了识别. 结果表明，U71Mn钢轨在冷焊的工艺下，热影响区内会产生裂纹，显微组织为马氏体组织. 随着预热和后热温度的提高，马氏体组织的消除效果越加明显. 当预热温度为320 ℃，后热温度为550 ℃时可以完全避免热影响区内马氏体组织的形成，生成比母材珠光体晶粒细小的索氏体组织，热影响区的硬度分布均匀.

关键词：动态感应加热；U71Mn钢轨；堆焊；马氏体组织
中图分类号：TG 401 **文献标识码**：A **文章编号**：0253－360X(2014)11－0097－04

0 序 言

由钢轨轨面生锈造成的轨道电路分路不良会给铁路交通带来巨大的安全隐患. 针对这一问题，采用轨面堆焊不锈钢焊道的方案使车轮与轨道之间形成良好的导电通路. 然而钢轨碳含量高，淬火硬化倾向大，在堆焊过程中极易产生马氏体组织，是钢轨在焊后产生断裂的主要原因之一[1,2]. 因此钢轨轨面堆焊不锈钢，必须对堆焊热影响区组织进行控制，确保堆焊后钢轨的质量.

通过有效的预热和后热方式控制焊后冷却速度被认为是解决高碳钢焊后形成马氏体组织最为理想的方法[3,4]. 赵敏海[5]采用不同的预热温度和冷却方式对钢轨焊接金相显微组织进行了观察，结果表明焊前预热，焊后炉中缓冷或石棉布保温缓冷可以消除马氏体组织. 但是炉中缓冷并不适用于现场进行轨面堆焊，而采用石棉布缓冷的方法需要分配专门的工人进行铺盖，工作效率低且如果铺盖的不及时同样会造成淬硬马氏体组织的产生，质量不稳定.

针对上述问题，文中采用动态感应加热的方法对钢轨堆焊进行预热和后热，达到消除母材热影响区马氏体组织的目的. 该工艺将预热、焊接和后热过程一次性完成，方便快捷，节省劳动力而且提高了工作效率.

1 动态感应加热消除马氏体组织原理

动态感应加热消除焊接淬硬组织的核心思想为利用一个特殊绕制的前后一体的感应加热线圈对钢轨进行焊前预热和焊后后热. 为避免线圈对焊枪的影响，将焊枪固定在前后线圈中间位置，并与线圈同步行走，如图1a所示. 钢轨轨面堆焊时，预热线圈对钢轨轨面进行预热，在一定程度上减缓其冷却速度. 焊接后，后热线圈立即对钢轨轨面进一步加热，

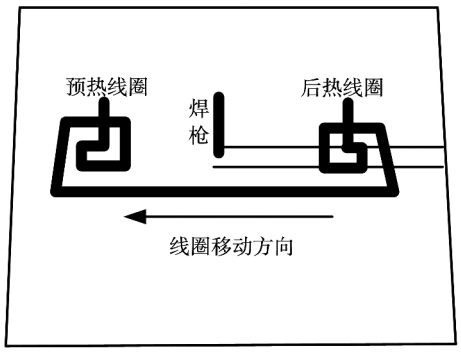

(a) 动态感应加热示意图

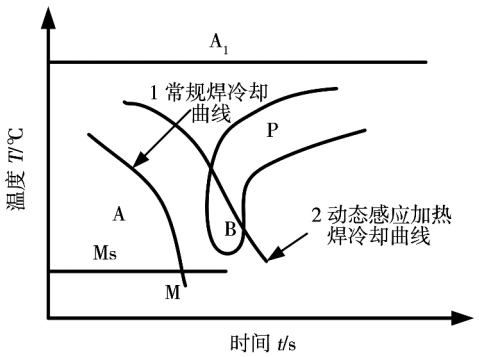

(b) 动态感应加热冷却曲线示意图

图1 动态感应加热消除马氏体组织原理图

Fig. 1 Schematic of inhibiting formation of martensite structure using dynamic induction heating

收稿日期：2013－06－27

在预热和后热的双重作用下控制焊接热循环过程的冷却曲线，使焊后工件的冷却曲线由图1b中的曲线1绕过工件的马氏体生成区间转变为曲线2，抑制淬硬马氏体组织的形成，从而达到避免马氏体组织形成的目的.

2 试验材料与试验方法

2.1 试验材料

试验所选用的钢轨型号为中国目前主干线铁路大量使用的U71Mn钢轨，其化学成分见表1.

2.2 试验方法

为了确定U71Mn钢轨堆焊所需要的最佳预热温度和后热温度组合，试验分别选取五组试样进行比较分析. 首先在不进行焊接的情况下，对钢轨进行动态感应加热，采用德国IMPAC红外测温仪对预热温度和后热温度进行测温(两线圈中间位置即焊枪处温度视为预热温度). 之后在室温不低于20 ℃下采用MIG焊的方法以相同的焊接工艺参数对不同预热/后热温度下的试样进行堆焊试验. 钢轨堆焊前应清除待焊部位轨面油污与铁锈，使之露出金属光泽. 焊接工艺参数见表2，不同预热、后热温度组合见表3.

表1 U71Mn钢轨化学成分(质量分数，%)

Table 1 Chemical compositions of U71Mn rail steel

钢号	C	Si	Mn	P	S	V	Nb	Fe
U71Mn	0.65～0.76	0.15～0.35	1.10～1.40	≤0.030	≤0.030	≤0.030	≤0.010	余量

表2 焊接工艺参数

Table 2 Welding parameters

焊丝直径 d/mm	气体流量 q/(L·min^{-1})	焊接电流 I/A	电弧电压 U/V	焊接速度 v/(mm·min^{-1})	焊丝伸出长度 L/mm
1.2	16～18	140	28	360	12～15

表3 不同预热/后热温度组合

Table 3 Samples heated at different temperatures

试样编号	预热温度 T_1/℃	后热温度 T_2/℃
A	0	0
B	190	480
C	200	550
D	290	500
E	320	550

焊后各组试样经过线切割、镶样、研磨、抛光和4%的硝酸酒精腐蚀，制成金相试样. 采用OLYMPUS BX51M金相显微镜观察焊接热影响区的金相组织. 在HXD1000硬度测试仪上测试焊接热影响区的维氏显微硬度，测试部位以焊接熔合线处为起始点，每隔0.1 mm取一个测试点，直到母材为止. 记录下每个测试点的硬度值，绘制出维氏硬度分布曲线，加载力为1 N，持续时间为10 s.

3 试验结果

3.1 焊接热影响区金相组织分析

图2为冷焊工艺条件下(试样A)母材热影响区的金相显微组织. 从图2a中可以观察到整个热影响区几乎全部都是亮白的马氏体组织. 由于先形成的马氏体组织较长且易被腐蚀液侵蚀，后形成的马氏体较短且相对来说不易被腐蚀液侵蚀，因此在过热区可以观察到大小不同、颜色深浅不一的针状马氏体组织，如图2b所示. 而靠近母材侧的正火区内，尤其是正火区的低温一侧，由于成分偏析及加热影响小的缘故，保留了少量的珠光体组织，如图2c所示.

在热影响区内出现走向与熔合线近乎平行的焊道下裂纹. 该裂纹的形成主要是由于钢轨轨面堆焊过程中，不均匀的热输入导致在热影响区附近出现拉应力峰值，钢轨本身含碳量高，淬硬倾向大，在冷却速度过快的条件下极易形成马氏体组织，发生马氏体相变，产生较大的相变应力，它与热应力共同作用容易使得堆焊金属开裂[6]. 此外从金属强度理论可以知道马氏体是一种非常硬脆的组织，发生断裂时只消耗较低的能量，本身又具有大量的晶格缺陷，如空位、位错等. 因此当焊接接头有马氏体存在时，裂纹就易于形成和扩展[7].

图3为不同预热温度和后热温度下轨面堆焊热影响区的金相显微组织. 从马氏体组织生成的部位来看，靠近熔合线侧的过热区由于冷却速度过快，更易形成淬硬的马氏体组织(其中亮白色部分). 从马氏体产生的数量来看，随着预热/后热温度的升高，

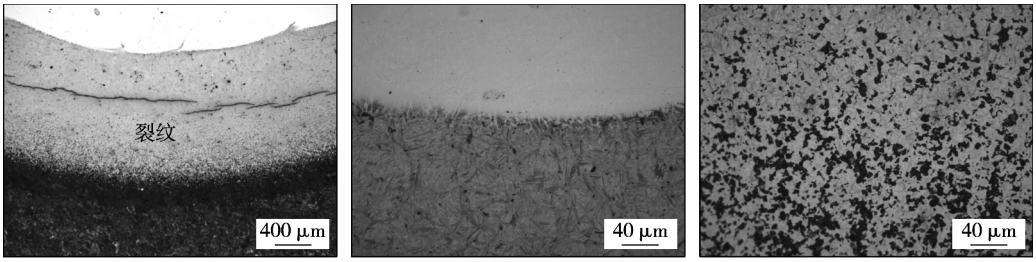

(a) 热影响区组织全貌　(b) 过热区组织　(c) 正火区组织

图 2　试样 A 热影响区显微组织

Fig. 2　Microstructure of heat affected zone of sample A

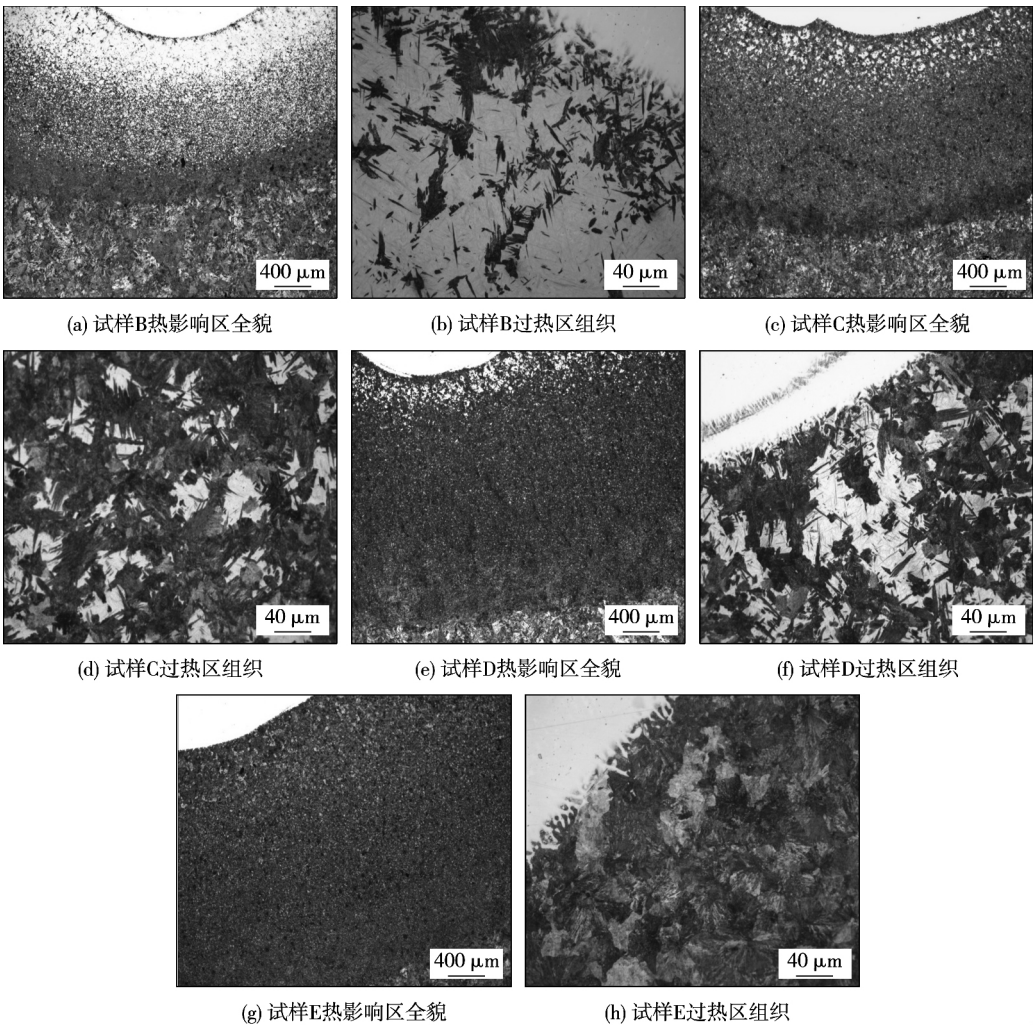

(a) 试样B热影响区全貌　(b) 试样B过热区组织　(c) 试样C热影响区全貌

(d) 试样C过热区组织　(e) 试样D热影响区全貌　(f) 试样D过热区组织

(g) 试样E热影响区全貌　(h) 试样E过热区组织

图 3　不同预热/后热温度下试样热影响区组织形貌

Fig. 3　Microstructure of heat affected zone of samples at different temperatures

马氏体数量明显减少. 各组试样热影响区内均未有裂纹的产生. 表明，通过预热和后热处理，可以预防钢轨热影响区内的焊道下裂纹的产生. 图 4 为试样 E 正火区组织形貌. 图 5 为试样 E 母材正常组织形貌.

从图 3h，图 4，图 5 对比可以看出，此工艺条件下，未发现明显的马氏体组织. 在热影响区中过热区一侧的珠光体晶粒尺寸较大，正火区的珠光体晶粒尺寸较小，但整个热影响区的珠光体比母材晶粒细小. 由于焊接时过热区金属处于过热状态，加之预热也会使其在高温阶段停留时间加长，奥氏体晶粒发生长大现象，冷却后得到较为粗大的组织. 而正火区处于 A_{C_1} ~1 000 ℃之间的温度范围，奥氏体化的晶粒细小，因此冷却至室温后获得相对细小均

匀的索氏体组织.

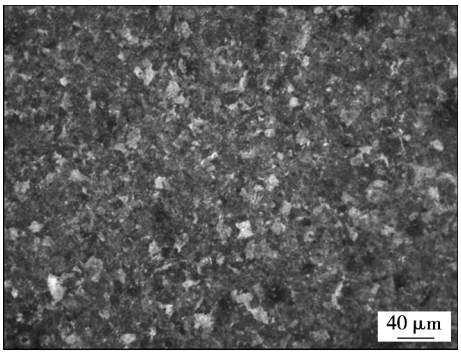

图 4 试样 E 正火区组织形貌

Fig. 4 Microstructure of normalized zone of sample E

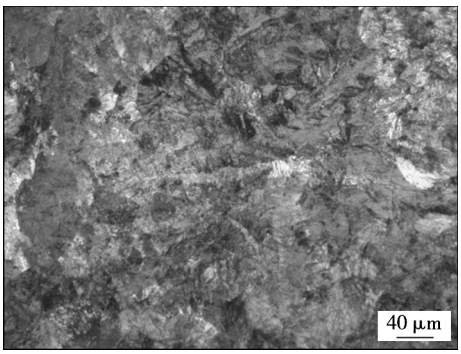

图 5 试样 E 母材正常组织形貌

Fig. 5 Microstructure of base metal of sample E

热影响区珠光体晶粒相对母材细小的原因是由于在预热 320 ℃、后热 550 ℃的工艺下,冷却速度相对来说依旧较快,而过冷奥氏体连续冷却转变为珠光体组织时,冷却速度越大,转变温度越低,所得的珠光体组织的片层间距越细[8].

3.2 显微硬度分析

对 5 组试样热影响区分别进行了显微硬度测试分析,结果如图 6 所示. 试样 A 整个热影响区的硬度值均很高,最大硬度值高达 1 000 MPa 以上,仅在靠近母材侧的硬度值相对较低. 试样 B 则在熔合线附近硬度值较高,随着距熔合线距离的增加,硬度值有所下降,在靠近母材侧硬度值降低并趋于平稳. 试样 C 和试样 D 则分别在距熔合线约为 0.4 mm 和 0.2 mm 处出现高硬度值,在远离熔合线处的热影响区硬度值趋于稳定. 试样 E 在整个热影响区内均未出现高硬度值,硬度值分布均匀,维持在 330 MPa 左右. 以上现象的出现与热影响区内的显微组织有很大的关系. 由于焊接热循环过程中,熔合线附近的过热区较母材侧的正火区更易形成高硬度的马氏体组织,而随着距熔合线距离的增加,冷却速度降低,在一定的预热/后热温度下则抑制了高硬度马氏体组织的生成,取而代之的是转变成低硬度值的珠光体组织. 试样 E 整个热影响区内均未出现高硬度值,说明该工艺下热影响区内未生成高硬度的马氏体组织.

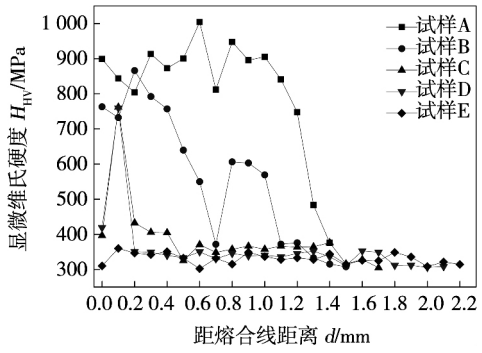

图 6 试样热影响区显微硬度分布曲线

Fig. 6 Microhardness distribution curves of samples

通过对不同试样金相组织和显微硬度的对比分析,可知随着预热和后热温度的提高,热影响区内马氏体组织转变量明显减少,且预热和后热的温度越高,对马氏体组织的消除越有利. 动态感应加热消除马氏体组织的方案是行之有效的. 当预热温度为 320 ℃,后热温度为 550 ℃时可以避免马氏体组织的形成.

4 结 论

(1) U71Mn 钢轨在冷焊的工艺下进行堆焊,会在热影响区内直接产生平行于熔合线的裂纹,显微组织为粗大的针状马氏体组织.

(2) 采用动态感应加热消除钢轨堆焊热影响区的马氏体组织是行之有效的. 随着预热和后热温度的提高,马氏体组织消除的效果越明显. 当预热温度和后热温度分别为 320 ℃和 550 ℃时,可以避免热影响区内高硬度马氏体组织的形成.

(3) 经过动态感应加热后的 U71Mn 钢轨焊接热影响区内的显微组织为比母材珠光体晶粒细小的索氏体组织.

参考文献:

[1] 邓建辉. 75 kg/m 热处理钢轨断裂原因分析[J]. 理化检验-物理分册, 2005, 41(4): 195-198.
Deng Jianhui. Fracture analyse of the 75 kg/m heat-treatment rail [J]. Ptca (Part: a Phys. Test), 2005, 41(4): 195-198.

[下转第 108 页]

4 结 论

(1) 在陶瓷封装结构中,依据不同表面缺陷类型及危险程度不同这一特性,可以通过接头结构的设计来提高钎焊工艺的可靠性. .

(2) 在陶瓷金属钎焊接头的结构优化中,可以将高应力转移到无脆性缺陷的金属化的上表面来避免失效的发生,最优化的结构参考陶瓷结构上表面和侧面的第一主应力差值进行选择.

参考文献:

[1] Fabis P M. Reliability of radio frequency/microwave power packages: the effects of component materials and assembly processes [J]. Microelectronics Reliability, 1999, 39(8): 1265 - 1274.

[2] 龚江宏. 陶瓷材料断裂力学 [M]. 北京: 清华大学出版社有限公司, 2001.

[3] 冯广杰, 李卓然, 徐 慨, 等. SiC 陶瓷真空钎焊接头界面结构及机理分析 [J]. 焊接学报, 2014, 35(1): 13 - 16.
Feng Guangjie, Li Zhuoran, Xu Kai, *et al*. Interface microstructure and mechanism of SiC vacuum brazed joint [J]. Transactions of the China Welding Institution, 2014, 35(1): 13 - 16.

[4] ANSYS 高级工程有限元分析范例精选 [M]. 北京: 电子工业出版社, 2004.

[5] Barlow Ⅲ, Fred, Aicha Elshabini. Ceramic interconnect technology handbook [M]. Florida: The Chemical Rubber Company Press, 2010.

作者简介: 曾 超,男,1982 年出生,博士研究生. 主要陶瓷封装可靠性的研究工作. 发表论文 10 余篇. Email: zchao808@hotmail.com

[上接第 100 页]

[2] 宴建武, 王伟兰, 艾云龙, 等. U71Mn 干线钢轨开裂原因及热处理工艺分析 [J]. 南昌航空工业学院学报, 2001, 15(4): 38 - 41.
Yan Jianwu, Wang Weilan, Ai Yunlong, *et al*. Analysis of quenching techniques and cracking of the end of U71Mn rail [J]. Journal of Nanchang Institute of Aeronautical Technology, 2001, 15(4): 38 - 41.

[3] Zhang Fucheng, Lü Bo, Hu Baitao, *et al*. Flash butt welding of high manganese steel crossing and carbon steel rail [J]. Materials Science and Engineering, 2007, 454/455(4): 288 - 292.

[4] Bipin Kumar Srivastava, Tewari DR S P, Jyoti Prakash. A review on effect of preheating and/or post weld heat treatment (PWHT) on mechanical behaviour of ferrous metals [J]. International Journal of Engineering Science and Technology, 2010, 2(4): 625 - 631.

[5] 赵敏海, 郭面焕, 董卫国, 等. 重型钢轨与高锰钢辙叉的焊接 Ⅱ [J]. 焊接学报, 2002, 23(4): 9 - 12.
Zhao Minhai, Guo Mianhuan, Dong Weiguo, *et al*. Welding of railway and high manganese steel frog Ⅱ [J]. Transactions of the China Welding Institution, 2002, 23(4): 9 - 12.

[6] 李 达, 高 军, 张运坤, 等. 马氏体相变对中高碳钢堆焊冷却过程内应力场的影响 [J]. 北京科技大学学报. 2006, 28(1): 526 - 528.
Li Da, Gao Jun, Zhang Yunkun, *et al*. Martensite transformation effects on the internal stress field of medium-high carbon steel during hardfacing cooling process [J]. Journal of University of Science and Techonlogy Beijing, 2006, 28(1): 526 - 528.

[7] 张文钺. 焊接冶金学(基本原理) [M]. 北京: 机械工业出版社, 1966.

[8] 王 贵, 麻永林, 王宝峰, 等. U71Mn 钢 CCT 曲线测定及连续冷却转变研究 [J]. 包头钢铁学院学报, 1995, 14(3): 41 - 44.
Wang Gui, Ma Yonglin, Wang Baofeng, *et al*. The study on CCT diagram and continuous cooling transformation of U71Mn steel [J]. Journal of Baotou University of Iron and Steel Technology, 1995, 14(3): 41 - 44.

作者简介: 兖文涛,男,1987 年出生,硕士研究生. 主要从事焊接及表面工程研究. 发表论文 2 篇. Email: wentao9836@126.com

通讯作者: 李晓延,男,教授,博士研究生导师. Email: xyli@bjut.edu.cn

Abstract: In order to understand the corrosion resistance of different materials surfaces machined by micro wire electrical discharge machining (MWEDM), the specimens of three kinds of materials, including W18Cr4V, 60Si2Mn and M42, were separately processed. The micro electrolytic cell equipment and electrochemical workstation were applied to test the corrosion resistance of specimen surfaces, and the electrochemical impedance spectroscopy and potentiodynamic polarization curves were measured and analyzed. Besides, the surfaces after corrosion were observed with inverted metallurgic microscope, and were compared to flat grinding surfaces. The results showed that corrosion resistance of MWEDM surfaces was superior to that of flat grinding surfaces. For different materials, corrosion resistance of MWEDM surfaces was significantly different from each other. For the same material, the surface with better corrosion resistance could be obtained by using appropriate processing parameters.

Key words: micro wire electrical discharge machining; corrosion resistance; electrochemical impedance spectroscopy; potentiodynamic polarization curve

Using dynamic induction heating to inhibit martensite structure formed in heat-affected zone of U71Mn steel rail after surface welding YAN Wentao, LI Xiaoyan, LI Hui, SUN Jiantong (School of Material Science and Engineering, Beijing University of Technology, Beijing 100124, China). pp 97 – 100, 108

Abstract: A dynamic induction heating method was used to inhibit the formation of martensite in heat-affected zone (HAZ) of U71Mn steel rail after surface welding. The inhibition of martensite structure was characterized by optical microstructure analysis and microhardness testing. The experimental results showed that when the U71Mn steel rail was welded in cold welding condition, cracks would form directly in the heat-affected zone, and the microstructure was martensite. With the increase of preheating and post-heating temperature, the amount of martensite reduced significantly. When the preheating temperature was 320 ℃ and post-heating temperature was 550 ℃, the martensite structure could be inhibited completely, and the heat-affected zone consisted of sorbite structure whose size was smaller than pearlite structure in the base metal. The microhardness of the heat-affected zone also distributed uniformly.

Key words: dynamic induction heating; U71Mn steel rail; surface welding; martensite

Arc pressure analysis in variable polarity TIG welding CHENG Lin, HU Shengsun, WANG Zhijiang (Tianjin Key Laboratory of Advanced Joining Technology, Tianjin University, Tianjin 300072, China). pp 101 – 104

Abstract: The arc pressure during horizontal variable polarity gas tungsten arc welding (VPTIG) was measured by pressure transducer under different welding conditions. The radial distribution of arc pressure was investigated, and the central arc pressures for DC TIG welding and VPTIG welding with a period of 5% and 15% for direct current electrode positive (DCEP) were compared. The experimental results showed that the radial distribution of VPTIG pressure was hyperbolic. When the welding current was in the range of 100 A to 140 A and with the same root mean square value, the arc pressure decreased gradually with the increase of time ratio of DCEP at one cycle during DC TIG welding and VPTIG welding with a period of 5% and of 15% for DCEP, due to the difficulties of electron emission and arc divergence in the period of DCEP. And the integrated arc force was directly proportional to the square of welding current.

Key words: hyperbolic distribution; arc pressure; horizontal welding; variable polarity gas tungsten arc welding

Effect of hot-cutting defect on reliability of brazing process in ceramic package manufacturing——II. Brazing structure design ZENG Chao, WANG Chunqing, TIAN Yanhong, ZHANG Wei (State Key Lab of Advanced Welding and Joining, Harbin Institute of Technology, Harbin 150001, China). pp 105 – 108

Abstract: Reliability of brazing process in ceramic package manufacturing depends on the interaction between thermal stress induced by mismatch of CTE (coefficient of thermal expansion) and defect in ceramic generated in the process before brazing. This paper based on the feature that defects with different degrees of danger spatially locate differently, and employed ANSYS software to analyze the distribution of the thermal stress in brazing process. A novel idea of avoiding the stress locating at defect region was applied to improve the reliability of assembly process. This idea is different from the traditional optimizing method to lowering the stress over the whole component, and is more flexible for the package design, and it is also more effective for improving the reliability of ceramic package manufacturing.

Key words: thermal mismatch; package structure; process reliability

Finite element numerical simulation of electron beam welding of TC4 titanium alloy ZENG Qingji[1], XU Lianyong[1,2], HAN Yongdian[1,2], JING Hongyang[1,2], ZHOU Chunliang[3] (1. School of Materials Science and Engineering, Tianjin University, Tianjin 300072, China; 2. Tianjin Key Laboratory of Advanced Joining Technology, Tianjin 300072, China; 3. The 18th Research Institute of CETC, Tianjin 300381, China). pp 109 – 112

Abstract: The optimized welding parameters for electron beam welding of 9 mm thick TC4 titanium alloy plate were obtained. A finite element model was established based on ABAQUS software, and the simulated results of the weld appearance and residual stress on the weld surface agreed well with the experimental results. This proved that the combined heat source with highly penetrating cone heat source and highly irradiative dual-ellipsoid heat source could characterize the electron beam welding. Further simulated results showed that high residual stress occurred around the weld, especially, dangerous three-dimensional tensile stress existed within the weldment.

Key words: electron beam welding; TC4 titanium; finite element numerical simulation; residual stress; composite heat source